The operational cloud retrieval algorithms from TROPOMI on board Sentinel-5 Precursor

Diego G. Loyola[1], Sebastián Gimeno García[1], Ronny Lutz[1], Fabian Romahn[1], Robert J.D. Spurr[2], Mattia Pedergnana[1], Adrian Doicu[1], Olena Schüssler[1]

[1]German Aerospace Centre (DLR), Remote Sensing Technology Institute, Oberpfaffenhofen, 82234 Wessling, Germany
[2]RT Solutions, Inc. 9 Channing Street, Cambridge, MA 02138, USA

Correspondence to: Diego Loyola (Diego.Loyola@dlr.de)

Abstract. This paper presents the operational cloud retrieval algorithms for the TROPOspheric Monitoring Instrument (TROPOMI) on board the European Space Agency Sentinel-5 Precursor (S5P) mission scheduled for launch in 2017.

Two algorithms working in tandem are used for retrieving cloud properties: OCRA (Optical Cloud Recognition Algorithm) and ROCINN (Retrieval of Cloud Information using Neural Networks). OCRA retrieves the cloud fraction using TROPOMI measurements in the UV/VIS spectral regions and ROCINN retrieves the cloud top height (pressure) and optical thickness (albedo) using TROPOMI measurements in and around the oxygen *A*-band in the NIR.

Cloud parameters from TROPOMI/S5P will be used not only for enhancing the accuracy of trace gas retrievals, but also for extending the satellite data record of cloud information derived from oxygen *A*-band measurements, a record initiated with GOME/ERS-2 over twenty years ago. Use of the oxygen *A*-band generates complementary cloud information (especially for low clouds), as compared to traditional thermal infrared sensors (as used in most meteorological satellites) that are less sensitive to low clouds due to reduced thermal contrast.

The OCRA and ROCINN algorithms are integrated in the S5P operational processor UPAS (Universal Processor for UV/VIS/NIR Atmospheric Spectrometers), and we present here UPAS cloud results using OMI and GOME-2 measurements. In addition, we examine anticipated challenges for the TROPOMI/S5P cloud retrieval algorithms and we discuss the future validation needs for OCRA and ROCINN.

1. Introduction

Clouds are an important component of the hydrological cycle and play a major role in the Earth's climate system through their strong impact on radiation processes. The interplay of sunlight with clouds imposes major challenges for satellite remote sensing, both in terms of the spatial complexity of real clouds and the dominance of multiple scattering in radiation transport. The retrieval of trace gas products from TROPOMI/S5P will be strongly affected by the presence of clouds.

The physics behind the influence of cloud on trace gas retrieval is well understood, and in general, there are three different contributions (Liu et al., 2004; Kokhanovsky and Rozanov, 2008; Stammes et al., 2008; Wagner et al., 2008): (a) the albedo effect associated with the enhancement of reflectivity for cloudy scenes compared to cloud-free sky scenes, (b) the so-called shielding effect, by which that part of the trace gas column below the cloud is hidden by the clouds themselves, and (c) the

5 increase in absorption within the cloud, related to intra-cloud multiple scattering enhancements of optical path lengths. The albedo and in-cloud absorption effects increase the visibility of trace gases at and above the cloud top, while the shielding effect (if not corrected for) normally results in an underestimation of the trace gas column.

Using radiative transfer modelling, several papers have quantified the influence of cloud parameters on the retrieval of trace gas columns (Liu et al., 2004; Ahmad et al., 2004; Boersma et al., 2004; Van Roozendael et al., 2006; Kokhanovsky et al.,

10 2007; Doicu et al., 2014). These studies have shown that cloud fraction, cloud optical thickness (albedo), and cloud top pressure (height) are the most important quantities determining cloud correction of satellite trace gas retrievals.

TROPOMI (Veefkind et al., 2012) has eight spectral bands covering the UV, VIS, NIR, and SWIR spectral regions, and an unprecedented spatial resolution of 7x3.5 km² at nadir. It will fly on board S5P in a sun-synchronous polar orbit providing a daily global coverage with a wide swath of 2600 km. TROPOMI/S5P will be the first atmospheric composition mission of

15 the European Copernicus programme and TROPOMI's 7-year lifetime will extend the unique data record started more than 20 years ago with GOME/ERS-2, SCIAMACHY/ENVISAT, OMI/AURA, and GOME-2 (on board the MetOp-A and MetOp-B satellites).

This paper provides a detailed description of the operational TROPOMI/S5P cloud retrieval algorithms. We start with a short overview in Section 2. In Sections 3 and 4, we present the OCRA algorithm for the cloud fraction retrieval using TROPOMI

20 measurements in the UV/VIS spectral regions and the ROCINN algorithm for the retrieval of cloud top height (pressure) and optical thickness (albedo) using TROPOMI measurements in and around the oxygen A-band in the NIR. The error budget of the OCRA and ROCINN retrievals is described in Section 5 and results from application of the S5P algorithms to OMI and GOME-2 measurements are presented in Section 6. In Section 7, we discuss anticipated challenges for the TROPOMI/S5P cloud retrieval algorithms, and the future validation needs for OCRA and ROCINN.

25 ## 2. Overview of the Cloud Retrieval Algorithms

The operational TROPOMI/S5P cloud properties are retrieved using two algorithms working in tandem: OCRA and ROCINN.

OCRA derives the cloud fraction from UV/VIS radiances by separating the sensor measurements into two components: a cloud-free background and a remainder expressing the influence of clouds. OCRA was first developed for GOME/ERS-2 in

30 the late 1990s using data from GOME's broad-band PMDs (Polarization Measurement Devices). OCRA has also been applied operationally to SCIAMACHY and GOME-2. Initial cloud-free backgrounds for these sensors were based on GOME

data before dedicated measurements became available from SCIAMACHY and GOME-2. In this paper we present the adaptation of OCRA to TROPOMI/S5P using UV/VIS radiances themselves (instead of PMD measurements), with an initial cloud-free background based on OMI data.

ROCINN is based on the comparison of measured and simulated satellite sun-normalized radiances in and near the O_2 A-band to retrieve cloud height and cloud optical thickness. ROCINN uses the cloud fraction from OCRA as a baseline input. Two sets of TROPOMI/S5P cloud properties will be provided by ROCINN: (a) cloud top height and cloud top albedo using the "Clouds-as-Reflecting-Boundaries" (CRB) model in which clouds are treated as simple Lambertian surfaces; and (b) cloud top height and cloud optical thickness using a more realistic "Clouds-As-Layers" (CAL) model in which clouds are treated as optically uniform layers of light-scattering particles (water droplets).

In this paper we present for the first time the ROCINN_CAL algorithm. CAL is the preferred method for the relatively small TROPOMI/S5P ground pixels (7x3.5 km^2). The CRB approach works best with large pixels (Kokhanovsky et al., 2007) such as those from GOME (footprint 320x40 km^2), where different types of clouds are combined and errors on the cloud model are self-compensating. Furthermore CAL is more accurate than CRB for optically thin clouds (Rozanov and Kokhanovsky, 2004) and these kinds of clouds are the most frequent on a global scale. Studies have shown that for the smaller GOME-2 pixels, CAL retrieval produces more reliable cloud information than that from CRB (Sihler et al., 2015), not only with regard to the accuracy of the cloud parameters themselves, but also with respect to the effect of cloud parameter uncertainties on total ozone accuracy (Loyola et al., 2017).

The following subsection presents a short summary of the heritage algorithms used for retrieving cloud information from UV/VIS/NIR spectrometers.

2.1. Heritage Algorithms

Several cloud retrieval algorithms based on measurements in and around the O_2 A-band at 760 nm have been developed for the GOME-type of sensors: these include the ICFA (Initial Cloud Fitting Algorithm) (Kuze and Chance, 1994), FRESCO (Fast REtrieval Scheme for Clouds from the Oxygen A-band) (Koelemeijer et al., 2001, Wang et al., 2008), SACURA (Semi-Analytical CloUd Retrieval Algorithm) (Rozanov and Kokhanovsky, 2004), and ROCINN algorithms. These are all based on the Independent Pixel Approximation (IPA), which is the assumption that the "radiative properties of a single satellite 'pixel' are considered in isolation from neighbouring pixels" (definition of the American Meteorological Society). The IPA allows for the application of one-dimensional plane-parallel radiative transfer (RT) theory in the forward simulation of cloud-contaminated atmospheric scenarios.

The ICFA algorithm was used in the initial GOME data processing to derive the effective fractional cover. The FRESCO algorithm, also developed for GOME, is based on the calculation of transmittances (later, single scattering radiances) and it retrieves effective cloud fraction and cloud top pressure, assuming a fixed cloud albedo of 0.8. The SACURA algorithm was

Atmospheric
Measurement
Techniques
Discussions

Open Access

developed initially for the SCIAMACHY instrument and then modified to handle also GOME measurements (Lelli et al., 2012). SACURA uses semi-empirical formulae from asymptotic radiative transfer theory to retrieve cloud optical thickness, cloud top height, liquid water path and other parameters. The ROCINN algorithm (Loyola et al., 2007) is currently being used in the operational GOME and GOME-2 products and it retrieves as primary quantities the cloud top height and cloud
5   albedo.

The broad-band polarization measurements from GOME, SCIAMACHY and GOME-2 are used for computing cloud fraction; see for example OCRA (Loyola et al., 1998; Lutz et al., 2016) and HICRU (Grzegorski et al., 2006). Enhancements to these algorithms have been introduced in more recent years - see for example the detection of Sun glint effects (Loyola et al., 2011; Lutz et al., 2016).

10 There are three cloud-property algorithms in operational use for the OMI instrument (OMI has no O_2 A-band measurements). The first (OMCLDRR) uses the cloud screening effect on Fraunhofer filling signatures (due to inelastic rotational Raman scattering) in the region 346-354 nm to derive effective cloud fraction and cloud optical centroid pressure (Joiner and Vasilkov, 2006; Vasilkov et al., 2008; Joiner et al., 2012). This algorithm is based on the minimum Lambertian equivalent reflectivity (MLER) assumption. The second algorithm (OMCLDO2) uses reflectances in and around the O_2-O_2 absorption
15 band near 477 nm (Acarreta et al., 2004, Veefkind et al., 2016); DOAS-retrieved O_2-O_2 slant columns are compared with simulated look-up table entries to obtain effective cloud fraction and cloud pressure. The third algorithm (OMAERUV) derives aerosol optical depth and single scattering albedo (Torres et al., 2007) from radiances in the range 330–390 nm; the cloud fraction is computed as an intermediate step.

3.   OCRA

20 The OCRA cloud fraction determination is based on the comparison between cloud-contaminated measurements and corresponding measurements for the background (cloud-free) surface. A flow chart of the OCRA algorithm is given in Figure 1, and the algorithm steps are described in the following subsections.

A description of the OCRA algorithm and its application to GOME and GOME-2 data is given in (Loyola, 1998; Lutz et al., 2016). For the TROPOMI/S5P application, the new algorithm developments for OCRA are the adaptation to work with 2-
25 colour radiances using the UV/VIS spectra instead of the 3-colour PMD measurements in the UV/VIS/NIR region.

3.1.   GB-colour conversion

The OCRA colour-space approach can be applied with three colours (RGB space) or two colours (GB space or RG space). For a given location (x, y), we define the reflectance $\rho(x, y, \lambda_i)$ at wavelength range λ_i for the ground-cover projection of the measurement as:

30
$$\rho(x, y, \lambda_i) = \frac{\pi \cdot I(\lambda_i)}{E_0(\lambda_i) \cdot cos\theta_0},$$
(1)

4

where $I(\lambda_i)$ and $E_0(\lambda_i)$ denote the measured earthshine backscattered radiance and the solar irradiance respectively, and θ_0 is the solar zenith angle.

The reflectances used in this algorithm are derived from broad-band measurements of backscattered radiance and extra-terrestrial solar irradiance covering the spectral range of the Green-Blue (GB) colour system. The OCRA spectral ranges with TROPOMI/S5P are 405-495 nm for G and 350-395 nm for B.

3.2. OCRA cloud-free background

The core of the algorithm is the construction of a cloud-free composite of multi-temporal (time series of measurements over the same location) reflectances that is independent of atmosphere and solar and viewing angles. For the off-line creation of the cloud-free reflectance composites in the GB case, the GB reflectances are translated into normalized gb-colour space via the relations

$$g = \frac{\rho(x,y,\lambda_G)}{\sum_{i=GB} \rho(x,y,\lambda_i)}, b = \frac{\rho(x,y,\lambda_B)}{\sum_{i=GB} \rho(x,y,\lambda_i)}, \qquad (2)$$

If M is the set of n normalized multi-temporal measurements over the same location (x, y), then a cloud-free (or minimum cloudiness) pixel $gb_{CF} \in$ M is selected using the brightness criterion $\|gb_{CF} - W\| \geq \|gb_k - W\|$, for $k = 1, \cdots n$, where W is the *white point* (1/2, 1/2) in the gb-chromaticity diagram. Measurements under cloudy conditions are projected to the white point, and the measurement that is most distant from W is considered to be cloud-free. A cloud-free background is constructed by merging cloud-free reflectances $\rho_{CF}(\lambda_i)$ (corresponding to gb_{CF}) at all locations.

At the beginning of the TROPOMI/S5P mission, a monthly cloud-free background data set based on OMI measurements will be used (see Figure 2 for example).

3.3. Cloud fraction derivation

The radiometric cloud fraction f_c is determined by examining separations between measured GB reflectances and their corresponding cloud-free composite values:

$$f_c = min\left\{1, \sqrt{\sum_{i=GB} \alpha(\lambda_i)\max\{0, [\rho(\lambda_i) - \rho_{CF}(\lambda_i) - \beta(\lambda_i)]\}^2}\right\}. \qquad (3)$$

This equation expresses the distance between actual measurements and the corresponding cloud-free scene in colour-space. Scaling factors $\alpha(\lambda_{i=GB})$ define the upper limit for reflectances under fully cloudy conditions, while offsets $\beta(\lambda_{i=GB})$ account for aerosol and other radiative effects in the atmosphere and as a lower limit basically define the cloud free conditions. The $max\{\}$ and $min\{\}$ functions ensure that the cloud fraction is confined to the interval [0, 1].

The scaling and offset factors are determined off-line using representative daily satellite measurements (Lutz et al., 2016). The offsets are the histogram modes from the difference $\{\rho(\lambda_i) - \rho_{CF}(\lambda_i)\}$ and the scaling factors are the inverses of the 99th percentile of the cumulative histograms from the differences $\{\rho(\lambda_i) - \rho_{CF}(\lambda_i)\}^2$.

Atmospheric
Measurement
Techniques
Discussions

3.3.1. Sun glint detection

Direct sunlight reflected by the ocean surface may reach the satellite sensor, enhancing the measured signal in a manner which contaminates cloud effects. Sun-glint flagging was developed as a component of the operational OCRA algorithm (Loyola, 2011) for GOME-2/MetOp-A, and this treatment was further enhanced using the polarization Stokes fractions (Lutz et al., 2016). As TROPOMI does not provide polarization information, a simplified sun-glint correction will be used. First, those areas that might be affected by sun glint are marked using the viewing geometry conditions of the measurement:

$$v = \sqrt{(|\Theta_o - \Theta| - 2)^2 + (\varphi_o - \varphi - 180)^2} \, , \tag{4}$$

where Θ_o, Θ are the solar are and satellite zenith angles, and φ_o, φ are the solar and satellite azimuth angles (values are given in degrees). A sun-glint flag is set whenever the value of "marker" v is larger than a given threshold and when the UV reflectance ratio $\frac{R_{336\,to\,340}}{R_{331\,to\,335}}$ is above a certain threshold. These threshold values will be determined dynamically when real TROPOMI data becomes available; for now, the OMI threshold value of 45 and 1.08 will be used initially.

4. ROCINN

ROCINN is based on the comparison of measured and simulated radiances in and near the O_2 A-band for retrieving the cloud optical thickness, cloud height and albedo. A flow chart of the ROCINN algorithm is given in Figure 3; the algorithm steps are described in the following subsections.

Previous versions of the ROCINN algorithm for operational processing of GOME (Van Roozendael et al., 2006) and GOME-2 (Loyola et al., 2011) modelled clouds as simple Lambertian surfaces (ROCINN_CRB). The CRB approach was originally developed for GOME (footprint 320x40 km²), where different types of clouds are combined in the large satellite pixels and errors in the cloud model are compensated (Kokhanovsky et al., 2007), but the limitations of the CRB model are already noticeable with GOME-2 (footprint 80/40x40 km²). For TROPOMI/S5P, with significantly smaller ground pixels (footprint 7x3.5 km²), we have developed the more sophisticated ROCINN_CAL algorithm presented in this paper. In CAL, clouds are modelled as optically uniform layers – with this more physically realistic scenario, CAL is expected to be more accurate than CRB, especially for optically thin clouds (Rozanov and Kokhanovsky, 2004).

4.1. Wavelength recalibration

Before we describe ROCINN itself, we remark on the initial wavelength registration (see Figure 3). The wavelength grid of the measured solar irradiance E_0 is recalibrated using a high-resolution solar reference E_{sol} by first dividing the fitting window into sub-windows and computing for each sub-window j a wavelength shift $\Delta\lambda_j$ between $E_{0,j}$ and $E_{sol,j}$. The recalibrated grid is then established by applying (at each original wavelength point) a shift value computed from a polynomial fit through the $\Delta\lambda_j$ for the various sub-windows.

6

Note that during the inversion (see section 4.5) a wavelength shift for the earthshine spectrum is additionally fitted.

The sun-normalized radiance $R(\lambda)$ at wavelength λ is then defined as:

$$R(\lambda) = \frac{I(\lambda)}{E_0(\lambda)} ,$$ (5)

where $I(\lambda)$ and $E_0(\lambda)$ denote the measured earthshine backscattered radiance and solar irradiance spectra respectively, both
5   spectra being registered on the recalibrated solar irradiance grid as noted above.

4.2. ROCINN_CAL

For ROCINN with CAL (Clouds-As-Layers), the total sun-normalized radiance is taken to be a linearly-weighted sum of independent radiances R_s for the clear-sky scene and R_c^{CAL} for the cloud-filled scene, with the weighting expressed through the radiometric cloud fraction f_c. Both radiance contributions are calculated using standard one-dimensional radiative
10   transfer models.

The sun-normalized radiance for a cloudy scene is calculated with the cloud treated as a set of contiguous scattering layers with geometrical extent characterized by cloud top height Z_{ct} and cloud base height Z_{cb} (or alternatively the cloud geometrical thickness $H_c = Z_{ct} - Z_{cb}$). The entire cloud is optically uniform with cloud optical thickness τ_c and its scattering properties are determined through Mie-scattering calculations for water droplet particles (microphysical properties
15   are discussed below). In the IPA, we may write sun-normalized CAL simulated radiances R_{sim}^{CAL} as:

$$R_{sim}^{CAL}(\lambda) = f_c R_c^{CAL}(\lambda, \Theta, \tau_c, Z_{ct}, Z_{cb}, A_s, Z_s) + (1 - f_c)R_s(\lambda, \Theta, A_s, Z_s) .$$ (6)

Here, Θ denotes path geometry (solar and line-of-sight angles), with surface properties being the Lambertian albedo A_s and lower boundary height Z_s.

Radiances for clear-sky and cloudy scenarios are calculated using the VLIDORT radiative transfer (RT) code (*Spurr*, 2006),
20   at wavelengths in and adjacent to the O_2 A-band. Details of the radiative transfer model (RTM) calculations are given in section 4.4 below.

A complete data set of simulated sun-normalized radiance templates is created off-line for an appropriate range of viewing/solar geometries and surface geophysical scenarios, and for various combinations of cloud properties.

The inverse problem uses least-squares fitting with a generalized form of Tikhonov regularization (details in section 4.5).
25   Retrieval in the O_2 A-band with the 4-element state vector $\{\tau_c, Z_{ct}, Z_{cb}, f_c\}$ is an ill-posed problem that requires additional information in order to obtain an inverse solution, as there are only two degrees-of-freedom-of-signal (Schuessler et al., 2014). For ROCINN[CAL], the retrieval state vector is just $\{\tau_c, Z_{ct}\}$ for cloud optical thickness τ_c and height Z_{ct}, a fixed cloud geometrical thickness of one kilometre is assumed and the radiometric cloud fraction f_c is taken from OCRA.

4.3. ROCINN_CRB

ROCINN with CRB (Clouds-as-Reflecting-Boundary) assumes that clouds are treated as Lambertian reflectors. The sun-normalized CRB simulated radiances R_{sim}^{CRB} are defined as:

$$R_{sim}^{CRB}(\lambda) = f_c R_c(\lambda, \Theta, A_c, Z_c) + (1 - f_c) R_s(\lambda, \Theta, A_s, Z_s) .\qquad(7)$$

The retrieval state vector for ROCINN^{CRB} is $\{A_c, Z_c\}$ for cloud albedo A_c and cloud height Z_c; the radiometric cloud fraction f_c is again from OCRA.

4.4. Forward model

ROCINN is based on simulated sun-normalized radiances at wavelengths in and around the O_2 A-band. Two sets of radiance templates were calculated using the CRB and CAL models. The cloudy-scene sun-normalized radiances R_c^{CAL} were calculated for a multi-layer atmosphere including multiple-scattering in all layers. Mie scattering was used to generate cloud optical properties. Details may be found in (Schuessler et al., 2014).

Simulated sun-normalized radiances $R_{sim}(\lambda)$ are calculated using the vector VLIDORT multiple scattering multi-layer discrete ordinate RTM (Spurr, 2006); the desired total intensity I will incorporate the effects of polarization. In addition to the cloud layers, VLIDORT calculations are based on clear sky optical properties for line absorption by oxygen and Rayleigh scattering by air molecules.

For the line absorption, it is necessary to calculate line-by-line (LBL) radiances (typically at resolution 0.0025 wave number for the range 758-771 nm) using line-spectroscopic information for the O_2 A-band, before convolution with the sensor slit function.

The spectroscopic data is taken from the HITRAN 2012 database (released in June 2013). Absorption cross-sections are computed using LBL software from DLR (Schreier and Schimpf, 2001; Schreier, 2011), in which line absorption signatures are accurately modelled with the Voigt profile.

For Mie scattering calculations, we require microphysical properties; however, we have found that the use of water or ice properties has a relatively small impact on the O_2 A-band spectral region. In addition, we have found that the consistency of cloud models (e.g. CAL or CRB) used in both the cloud and UV/VIS trace gas retrievals is far more critical than the optical properties selected for the RTM simulations of the CAL templates.

The refractive index is taken to be 1.33 for water droplet clouds (no absorption). Droplets are assumed to be poly-dispersed according to the modified-Gamma size distribution function:

$$n(r) = C r^{-\alpha} \exp\left[-\frac{\alpha}{\gamma}\left(\frac{r}{r_c}\right)^{\gamma}\right],\qquad(8)$$

which is parameterized by the mode radius r_c in [um] and constants α and γ describing the shape of the distribution following (Hess et al., 1998). In Eqn. (8), C is the normalization constant.

8

Atmospheric
Measurement
Techniques
Discussions
Open Access
EGU

The cloud *macro-physical* properties (classifications of cloud top height and cloud geometrical thickness) are based on the tables in (Wang et al., 2000). Details of this algorithm prototype may be found in (Schuessler et al., 2014).

The line-by-line RT calculations in the O_2 *A*-band are computationally very demanding, and this precludes the deployment of on-line calls to VLIDORT during the processing of TROPOMI data. For this reason, RTM simulations for the range of S5P

5   viewing conditions are performed in advance. Node points for the RTM are created using a "smart sampling" technique (Loyola et al., 2016) that minimizes the number of calls to the RTM and at the same time optimally covers the input space. There are many millions of forward model calculations required; this process is done off-line and normally takes several weeks to complete. In the next step, the LBL simulations are convolved with the TROPOMI instrumental spectral response function and the resulting radiances are used to train a neural network that accurately approximates the RTM template

10   output. The node point generation, RTM simulation, and neural-network training is done using the smart sampling and incremental function learning technique (Loyola et al., 2016). The trained neural network that computes the O_2 *A*-band sun-normalized radiances is used in the UPAS operational environment, and this enables ROCINN retrievals to be done very quickly.

4.5. Inverse model

15   If **x** is the state vector $\{\tau_c, Z_{ct}, A_s, f_c\}$ comprising possible cloud parameters for retrieval, and **b** denotes a vector of auxiliary forward-model parameters (surface properties, viewing geometry, etc.), we write the measurement vector as $\mathbf{y}^\delta = \mathbf{F}(\mathbf{x}, \mathbf{b}) + \boldsymbol{\delta}$, where **F** is the forward model and $\boldsymbol{\delta}$ is the data error vector. The inverse problem defined by this equation is nonlinear and ill-posed, and regularization is required in order to obtain a solution with physical meaning. The degree to which the problem is ill-posed is partly characterized by the condition number $c(\mathbf{K}) = \gamma_{max}/\gamma_{min}$ of the Jacobian matrix $\mathbf{K} = d\mathbf{F}/d\mathbf{x}$, where

20   γ_{max} and γ_{min} are the largest and the smallest singular values of **K**, respectively.

In the form of Tikhonov regularization that we use here, the regularized solution $\mathbf{x}_\alpha^\delta$ minimizes the objective functional:

$$\mathfrak{F}_\alpha(\mathbf{x}, \mathbf{b}) = \tfrac{1}{2}\{\|\mathbf{F}(\mathbf{x}, \mathbf{b}) - \mathbf{y}\|^2 + \alpha\|\mathbf{L}(\mathbf{x} - \mathbf{x}_a)\|^2\} , \qquad (9)$$

Here, α denotes the regularization parameter, and **L** is the regularization matrix (Doicu et al., 2010). The functional is defined with the L_2 Euclidean norm. The minimizer for Eqn. (9) can be computed with Gauss-Newton methods.

25   In statistical inversion theory, the Bayesian approach or the optimal estimation method can be regarded as a stochastic version of Tikhonov regularization. The maximum *a posteriori* solution coincides with the Tikhonov solution when the state vector **x** and the noise vector $\boldsymbol{\delta}$ are Gaussian random vectors with covariance matrices $\mathbf{C_x} = \sigma_x^2 \mathbf{I}_n$ and $\mathbf{C_\delta} = \sigma^2 \mathbf{I}_m$ respectively, where σ_x and σ are the corresponding standard deviations, and $\mathbf{I}_n$ is the identity matrix of size *n*. In this case, the regularization parameter α is the ratio of these two variances, that is $\alpha = \sigma^2/\sigma_x^2$.

As noted above, the operational ROCINN algorithm with CAL (or CRB) retrieves two cloud parameters: the cloud top height and cloud optical thickness (or cloud albedo) with the *a priori* cloud fraction take from OCRA and the surface albedo from climatology, but the inverse framework is general enough to allow for other options. Note that the cloud fraction and the surface albedo are included in the state vector with a very strong regularization (i.e. only very small changes are allowed)

5   in order to improve the fitting. The state vector includes additionally a single wavelength registration shift parameter that takes care of the Doppler effect. The inverse model requires the partial derivatives of the radiances with respect to the state vector elements and these Jacobians are provided by the forward model.

Convergence is reached when either the residual $\|\mathbf{F}(\mathbf{x}, \mathbf{b}) - \mathbf{y}\|^2$ or incremental changes in the retrieved parameters $\Delta_{\mathbf{x}}$ are smaller than pre-defined values (defaults 5E-3 and 5E-5 respectively), or when the maximum number of iterations (default

10   50) is reached. The default value for the regularization parameter α is 1E-4.

4.6. Retrieval diagnostics

The equivalence between the Bayesian approach and the method of Tikhonov regularization enables us to analyze the information content of the signal with respect to the retrieved parameters in a stochastic framework (Schuessler et al., 2014). The degree of freedom for signal (DFS) is a measure of the number of independent pieces of information in the

15   measurement, and it gives the minimum number of parameters which can be used to define a state vector without loss of information. It is defined as the trace of the averaging kernel matrix, which represents the sensitivity of the retrieval to changes in the *true* state. The DFS can be computed as:

$$DFS = \Sigma_i^n \frac{\gamma_i^2}{\gamma_i^2 + \alpha},$$
(10)

where γ_i^2 are the singular values of the matrix $\mathbf{K}$.

20   Another useful criterion for the estimation of the retrieval quality is the Shannon information content (SIC), which is a measure of the incremental gain in information, defined as the entropy difference between the *a priori* and *a posteriori* states; the corresponding formula reads as:

$$SIC = \frac{1}{2}\Sigma_i^n \log\left(1 + \frac{\gamma_i^2}{\alpha}\right).$$
(11)

The accuracy of the regularized solution is represented by the mean square error matrix:

25   $$\boldsymbol{S_\alpha} = \varepsilon\left\{\left(\boldsymbol{x}^\dagger - \boldsymbol{x}_\alpha^\delta\right)\left(\boldsymbol{x}^\dagger - \boldsymbol{x}_\alpha^\delta\right)^T\right\} \approx (I_n - \boldsymbol{A_\alpha})\left(\boldsymbol{x}_\alpha^\delta - \boldsymbol{x}_a\right)\left(\boldsymbol{x}_\alpha^\delta - \boldsymbol{x}_a\right)^T(I_n - \boldsymbol{A_\alpha})^T + \sigma^2\boldsymbol{K}_\alpha^\dagger\boldsymbol{K}_\alpha^{\dagger T},$$
(12)

where $\boldsymbol{x}^\dagger$ is the exact solution or "true state", $\boldsymbol{x}_\alpha^\delta$ the regularized solution, $\boldsymbol{x}_a$ the a priori state vector, $\boldsymbol{A_\alpha}$ the averaging kernel matrix, $\boldsymbol{K}_\alpha^\dagger$ the generalized inverse, σ the noise standard deviation, α the regularization parameter and ε the expected

value operator. Further information on the mean square error matrix and Tikhonov regularization can be found in (Doicu et al., 2010).

4.7. Retrievals using synthetic spectra

In order to evaluate the performance of the ROCINN retrieval algorithm in TROPOMI/S5P, a data set of synthetic

5 TROPOMI measurements has been created. Synthetic spectra were computed using VLIDORT for a number of different scenarios characterised by various illumination and observation geometries, surface albedo and cloudiness, see Figure 4.

In general, these closed-loop ROCINN_CAL retrieval results are excellent; the cloud top-height results have no bias. The ROCINN_CRB retrieval was also applied to the same data set of synthetic spectra in order to obtain retrievals of the cloud height and cloud albedo. The results are shown in Figure 5, as expected the CRB cloud height is systematically below the

10 simulated cloud top-height with a median difference of 1.2 ± 0.4 km.

Figure 6 shows the correlation from ROCINN_CAL retrievals of cloud optical thickness and ROCINN_CRB retrievals of cloud albedo.

5. Error characterization

The accuracy of the operational TROPOMI/S5P cloud products retrieved using the OCRA and ROCINN algorithms is

15 dependent on a number of different error sources.

The most important sources of model parameter uncertainty in ROCINN are errors on the assumed values for cloud fraction and surface albedo. Associated cloud property retrieval errors due to this source are discussed in detail in (Schuessler et al., 2014). Summarizing these findings, the cloud top height and cloud optical thickness can be accurately retrieved, even when the cloud geometrical fraction is underestimated or overestimated by as much as 20-30%. On the other hand, the cloud

20 optical thickness retrievals are quite sensitive to uncertainty in the surface albedo. Less significant are ROCINN errors due to uncertainties in the choices of Mie-scattering particle size distribution parameters.

Errors due to forward-model uncertainty are the hardest to quantify, as these are due to sources such as mathematical discretization choices and physical simplifications. The most basic assumption is of course the use of a simplified 1-D radiative transfer model as mandated by the IPA. 3-D RTM of atmospheres with clouds is notoriously difficult and time-

25 consuming. With the relatively small TROPOMI spatial footprint, horizontal inhomogeneity in cloud fields will be an important consideration from both the geometrical and the radiation perspectives. Some results for a 3-D treatment with clouds have been reported using Monte-Carlo models (Marshak and Davis, 2005) and more recently using stochastic RTM methods (Doicu et al., 2014). A detailed analysis of the uncertainties induced by the assumption of IPA with 1-D RTM can be found in a recently published paper (Efremenko et al., 2016); this analysis is the first of its kind to quantify 3-D forward

30 model and retrieval errors in ozone and cloud properties derived from UVN measurements.

11

From the TROPOMI calibration exercise, results indicate that instrumental errors such as signal-to-noise and radiometric uncertainties in the UVN region are relatively small, although stray light issues were identified in the NIR band. Both the errors induced on retrieved cloud properties due to NIR straylight and the precise knowledge of the slit function response functions will be assessed when the instrument provides measurements from space.

5   ## 5.1. Co-registration inhomogeneity flag

An important source of error is the spatial mis-registration between the UV/VIS and NIR bands from TROPOMI. The combination of information from different spectral bands is not trivial, since the spatial regions covered by the ground pixels from different spectral bands do not match exactly. One method for combining information from different bands is by means of the TROPOMI co-registration mapping tables which contain the fractions of overlapping areas between the source and
10   target pixels. For combinations based on OCRA UV bands 3, 4, 5 and ROCINN NIR band 6, a static co-registration table suffices. However, this method implies a smoothing of the source band products.

In this regard, a cloud co-registration inhomogeneity flag (CCIF) will be included in the S5P cloud products. This is determined as follows. First, a cloud co-registration inhomogeneity parameter (CCIP) is defined as the weighted averaged gradient of cloud fractions:

15
$$CCIP_j = \frac{\sum_i \omega_{ij} |f_{ci} - f_{cj}|}{\sum_i \omega_{ij}}, \tag{13}$$

where the weights ω_{ij} correspond to the co-registration mapping values between UV bands (source, index i) and the NIR band (target, index j). The CCIF is defined as:

$$CCIF_j = CCIP_j > p, \tag{14}$$

where p is a fixed threshold which has been set to 0.4 as the baseline, following extensive testing using the Suomi-NPP
20   VIIRS cloud product resampled to the TROPOMI spatial grid.

6.   Application to OMI and GOME-2

The operational OCRA and ROCINN cloud algorithms presented in this paper have been fully implemented and tested in the TROPOMI/S5P operational processor UPAS under development at DLR. The resulting output files will follow the same netCDF format structure used for all the S5P L2 products. The main outputs are the cloud products retrieved with OCRA and
25   ROCINN_CAL, while the ROCINN_CRB retrievals are to be reported in the detailed results group. For more information, the reader is referred to the S5P Cloud Product User Manual (Pedergnana et al., 2016).

In this section we present the results obtained through application of the TROPOMI/S5P cloud algorithms implemented in UPAS to measurements from OMI and GOME-2.

Atmospheric
Measurement
Techniques
Discussions

6.1. OCRA cloud fraction from OMI

As part of the S5P project we have adapted the OCRA algorithm to the OMI sensor (the precursor of TROPOMI).

OMI is a nadir-viewing push-broom spectrometer observing solar backscatter radiation in the ultraviolet and visible wavelength range up to 500 nm (Levelt et al., 2006). The swath width is 2600 km on ground, constituting more than 60

5   across-track pixels. The highest spatial resolution of 13 x 24 km^2 (in normal mode) is achieved for the nadir pixels. OMI was launched in 2004 on the NASA Aura satellite platform.

The first step is the calculation of a monthly OCRA cloud-free background data set as described in section 3.2; this was based on 3.5 years of OMI measurements from January 2004 to June 2006. The OMI cloud-free background data set for the month of August is shown in Figure 2. Note that OMI is extremely stable with almost no instrument degradation - this

10   facilitates significantly the calculation of the OCRA cloud-free backgrounds.

Secondly, the scaling and offset factors are computed following the procedure described in section 3.3. The resulting scaling factors are $\alpha_B = 2.88$ and $\alpha_G = 2.14$, and the offset factors are $\beta_B = 0.0138$ and $\beta_G = 0.0180$.

6.1.1. Comparison with the MODIS and the operational OMI cloud products

The cloud products used in this comparison are:

15   • OMAERUV product provided by O. Torres. The cloud fraction is an ancillary product from the absorbing aerosol index algorithm using OMI radiances at 388 nm and 354 nm (Torres et al., 2007).

• OMCLDO2 product version 2.0, provided by P. Veefkind. The cloud fraction of this product is based on the OMI O_2-O_2 absorption feature around 477 nm (Veefkind et al., 2016).

• OMCLDRR product taken from the OMMYDCLD product version 003 (J. Joiner 2014, OMI/Aura and MODIS/Aqua

20   Merged Cloud Product 1-Orbit L2 Swath 13x24 km V003, Greenbelt, MD, USA, Goddard Earth Sciences Data and Information Services Center (GES DISC), Accessed 26 Oct 2016). This OMI cloud fraction is based on the filling-in of Solar Fraunhofer lines caused by rotational Raman scattering in the 346-354 nm range.

• MODIS product co-located to OMI footprints from the OMMYDCLD product version 003.

Figure 7 shows the global cloud maps obtained with OCRA, OMAERUV, OMCLDO2, and OMCLDRR from OMI

25   measurements on July 16th, 2005; the four algorithms generate similar cloud features.

A quantitative comparison of the zonal mean cloud fractions from OMI and those derived with MODIS is presented in Figure 8. The UV sensors are not sensitive to optically thick clouds and as expected, MODIS generates larger cloud fractions compared to those from OMI. The cloud fractions of OMCLDO2 and OMCLDRR are similar because both algorithms assume a fixed cloud albedo or reflectance of 0.8 for the retrieval, but overall the cloud albedo is significantly smaller and

30   therefore the retrieved cloud fractions are smaller than the MODIS geometrical cloud fractions. OCRA and OMAERUV on

the other hand do not need to assume a fixed cloud albedo, and their retrieved cloud fractions are larger than those from OMCLDO2 and OMCLDRR. OCRA and OMAERUV report cloud fraction values more representative of the radiometric cloud fraction measured by the instrument.

6.2. ROCINN cloud height and optical thickness from GOME-2

In preparation for S5P we have applied the ROCINN_CAL algorithm to GOME-2, and in this section we present for the first time the resulting cloud properties.

The Global Ozone Monitoring Experiment-2 (GOME-2) is a nadir-viewing optical spectrometer that senses Earth's backscattered radiance and solar irradiance at UV/VIS/NIR wavelengths in the range 240-790 nm (Munro et al., 2016). The nominal full GOME-2 swath has a width of 1920 km in the direction perpendicular to the flight direction and a single scan line has an extension of 40 km in the flight direction. The ground pixels have a spatial resolution of 80 x 40 km^2. In addition, broad-band Polarization Measurement Devices (PMD) provide an eight-fold higher spatial resolution, i.e. 10 x 40 km^2 for a selection of 15 spectral windows. Currently there are two GOME-2 operational sensors onboard the EUMETSAT MetOp-A and MetOp-B satellites launched in 2006 and 2012 respectively; both GOME-2 sensors are operated in tandem providing global measurements on a daily basis. A third GOME-2 sensor onboard MetOp-C will be launched in 2018.

The VLIDORT line-by-line RTM simulations described in section 4.4 are convolved with the GOME-2 instrumental spectral response functions and the results used to train a neural network that accurately approximates the O$_2$ A-band reflectances (Loyola et al., 2016). As noted in section 4.5, the ROCINN cloud top-height and optical thickness are retrieved using the Tikhonov inversion, taking as input the OCRA cloud fraction computed from the GOME-2 PMD measurements (Lutz et al., 2016).

6.2.1. Comparison with GOME-2 cloud products

Figure 9 shows the global cloud maps obtained with ROCINN_CAL and ROCINN_CRB from GOME-2A (GOME-2 on MetOp-A) measurements on July 1st, 2012. As expected from the retrievals with synthetic data (section 4.7) the cloud height retrieved using ROCINN_CRB is smaller than the cloud-top height retrieved using ROCINN_CAL; the CRB model retrieves the centroid of the cloud and not the cloud-top (Joiner et al., 2012)). The cloud optical thickness from ROCINN_CAL nicely correlates with the cloud albedo from ROCINN_CRB.

The histogram of differences between the GOME-2A cloud heights on July 1st, 2012 obtained with ROCINN_CAL and ROCINN_CRB is presented in Figure 10. The CRB model underestimates the cloud top height with a median difference of 0.92 ± 0.75 km. +/- These results are consistent with the retrievals using synthetic data from section 4.7.

7. Conclusions

We have presented the latest versions of the retrieval algorithms OCRA and ROCINN to be used for the generation of the operational TROPOMI/S5P cloud products: cloud fraction, cloud top height (pressure) and optical thickness (albedo).

In UPAS, a special effort has been directed to optimizing the run-time performance of the algorithms in order to cope with the "big data" expected from TROPOMI (around 21 million ground pixels daily, with 1.5 million pixels per orbit). The operational cloud retrievals are extremely fast and accurate: the OCRA cloud fraction is computed using a simple expression (Eqn. 3), while the time consuming part of generating a cloud-free composite is done off-line. Similarly the complex and computationally expensive line-by-line RTM calculations needed for the ROCINN retrieval of cloud top height and optical thickness are replaced by fast artificial neural networks trained using the smart sampling and incremental function learning technique (Loyola et al., 2016).

The OCRA and ROCINN algorithms are integrated in the S5P operational processor UPAS for the generation of near-real-time and off-line products. In this paper we have shown that UPAS cloud properties retrieved from OMI and GOME-2 measurements provide a good basis for anticipated retrievals from TROPOMI measurements themselves.

The algorithms presented in this paper will be used during the S5P commissioning phase. The operational TROPOMI cloud products will be validated using ground-based measurements of cloud radar and microwave radiometer instruments available in CloudNet stations, and using cloud products from VIIRS (Visible/Infrared Imager and Radiometer Suite) onboard the Suomi NPP (NPOESS Preparatory Project) satellite of NASA/NOAA; the S5P orbit will trail five minutes behind Suomi NPP.

A number of future algorithm developments are planned once the TROPOMI data becomes available after the S5P launch: the spatial mis-registration between the UV/VIS and NIR bands will be characterized and the possibility of a correction will be investigated, the effects of TROPOMI straylight in NIR on the cloud retrievals will be analysed, and a cloud-free background data set based on TROPOMI/S5P when one full year of measurements becomes available will be generated; this will replace the initial cloud-free background data based on OMI.

The OCRA and ROCINN cloud parameters will be used for enhancing the accuracy of the operational TROPOMI/S5P trace gas products total ozone (Loyola et al., 2017), formaldehyde, and sulphur dioxide (Theys et al., 2016). OCRA and ROCINN will be also used for the generation of operational cloud products from the geostationary Copernicus atmospheric composition mission Sentinel-4 (S4). In this way, cloud products from atmospheric composition missions S5P and S4 will be consistent, and together they will extend for the next two decades the unique UVN cloud data record (Loyola et al., 2010) initiated over twenty years ago with GOME/ERS-2.

Atmospheric
Measurement
Techniques
Open Access
Discussions
EGU

References

Acarreta, J.R., J.F. de Haan and P. Stammes, Cloud pressure retrieval using the O2-O2 absorption band at 477 nm, J. Geophys. Res., 109, doi:10.1029/2003JD003915, 2004.

Ahmad, Z., Bhartia, P. K., and Krotkov, N.: Spectral properties of backscattered UV radiation in cloudy atmospheres, J. Geophys. Res , 109, D01201, doi:10.1029/2003JD003395, 2004.

Boersma K., Eskes, H., and Brinksma E.: Error analysis for tropospheric NO2 retrieval from space, J. Geophys. Res, 109, no. D4, 4311, DOI:10.1029/2003JD003 962, 2004.

Doicu, A, Efremenko, D., Loyola, D., and Trautmann, T.: Discrete ordinate method with matrix exponential for stochastic radiative transfer in broken clouds, J. Quant. Spectrosc. Radiat. Trans., in press, 2014.

Doicu, A., Trautmann, T., and Schreier, F.: Numerical Regularization for Atmospheric Inverse Problems, Berlin:Springer Verlag, 2010.

Efremenko, D. S., Schüssler, O., Doicu, A., and Loyola, D.: A stochastic cloud model for cloud and ozone retrievals from UV measurements, J. Quant. Spectrosc. Radiat. Transfer, 184, 167–179, doi:10.1016/j.jqsrt.2016.07.008, 2016.

Grzegorski, M., Wenig, M., Platt, U., Stammes, P., Fournier, N., and Wagner, T.: The Heidelberg iterative cloud retrieval utilities (HICRU) and its application to GOME data, Atmos. Chem. Phys., 6, 4461-4476, 2006.

Hess, M., P. Koepke, and I. Schult, Optical Properties of Aerosols and Clouds: The Software Package OPAC, Bull. Am. Met. Soc, 79, Issue 5, 1998.

Atmospheric
Measurement
Techniques
Discussions

Heue, K.-P., Coldewey-Egbers, M., Delcloo, A., Lerot, C., Loyola, D., Valks, P., and van Roozendael, M.: Trends of tropical tropospheric ozone from 20 years of European satellite measurements and perspectives for the Sentinel-5 Precursor, Atmos. Meas. Tech., 9, 5037–5051, doi:10.5194/amt-9-5037-2016, 2016.

Joiner, J., Vasilkov, A. P., Gupta, P., Bhartia, P. K., Veefkind, P., Sneep, M., de Haan, J., Polonsky, I., and Spurr, R.: Fast simulators for satellite cloud optical centroid pressure retrievals; evaluation of OMI cloud retrievals, Atmos. Meas. Tech., 5, 529-545, doi:10.5194/amt-5-529-2012, 2012.

Joiner, J., and A. P. Vassilkov, First results from the OMI rotational Raman scattering cloud pressure algo-rithm, IEEE Trans. Geosci. Remote Sens., 44, 1272–1282, 2006.

Koelemeijer, R., and P. Stammes, A fast method for retrieval of cloud parameters using oxygen A-band measurements from the Global Ozone Monitoring Experiment, J. Geophys. Res., 106, 3475-3490, 2001.

Kokhanovsky, A. A., and Rozanov V. V.: The uncertainties of satellite DOAS total ozone retrieval for a cloudy sky, Atmos. Res., 87, 27–36, doi:10.1016/j.atmosres.2007.04.006, 2008.

Kokhanovsky, A. A., Mayer, B., Rozanov, V. V., Wapler, K., Lamsal, L. N., Weber, M., Burrows, J. P., and Schumann, U.: The influence of broken cloudiness on cloud top height retrievals using nadir observations of backscattered solar radiation in the oxygen A-band, J. Quant. Spectrosc. Radiat. Transfer, 103, 460–477, doi:10.1016/j.jqsrt.2006.06.003, 2007.

Kuze, A., and K. V. Chance (1994), Analysis of Cloud-Top Height and Cloud Coverage from Satellites Using the O_2 A and B Bands, J. Geophys. Res., 99, 14481-14491.

Lelli, L., Kokhanovsky, A.A., Rozanov, V.V., Vountas, M., Sayer, A.M., and Burrows, J.P.: Seven years of global retrieval of cloud properties using space-borne data of GOME, Atmos. Meas. Tech., 5, 1551-1570, doi:10.5194/amt-5-1551-2015, 2012.

Levelt, P. F., van den Oord, G. H. J., Dobber, M. R., Malkki, A., Visser, H., de Vries, J., Stammes, P., Lundell, J. O. V., and Saari, H.: The Ozone Monitoring Instrument, IEEE T. Geosci. Remote Sens., 44, 1093–1101, 2006.

Liu, X., Newchurch, M., Loughman, R., and Bhartia P.K.: Errors resulting from assuming opaque Lambertian clouds in TOMS ozone retrieval, J. Quant. Spectrosc. Radiat. Transfer, 85, 337–365, 2004.

Loyola, D., et al.: The near-real-time total ozone retrieval algorithm from TROPOMI onboard Sentinel-5 Precursor, Atmos. Meas. Tech. Discuss., in preparation, 2017.

Loyola D., M. Pedergnana, S. Gimeno García, Smart sampling and incremental function learning for very large high dimensional data, Neural Networks, 78, 75–87, 2016.

Atmospheric
Measurement
Techniques
Discussions

Loyola, D., M. Koukouli, P. Valks, D. Balis, N. Hao, M. Van Roozendael, R. Spurr, W. Zimmer, S. Kiemle, C. Lerot, and J-C. Lambert, The GOME-2 Total Column Ozone Product: Retrieval Algorithm and Ground-Based Validation, J. Geophys. Res., 116, D07302, doi:10.1029/2010JD014675, 2011.

Loyola, D., W. Thomas, R. Spurr, B. Mayer, Global patterns in daytime cloud properties derived from GOME backscatter UV-VIS measurements, Int. J. Remote Sensing, 31(16), 4295-4318, doi: 10-1080/01431160903246741, 2010.

Loyola, D., W. Thomas, Y. Livschitz, T. Ruppert, P. Albert, and R. Hollmann, Cloud properties derived from GOME/ERS-2 backscatter data for trace gas retrieval, IEEE Trans. Geosci. Remote Sens., 45(9), 2747–2758, 2007.

Loyola, D., and T. Ruppert, A new PMD cloud-recognition algorithm for GOME, ESA Earth Observation Quarterly, 58, 45-47, 1998.

Lutz, R., Loyola, D., Gimeno García, S., and Romahn, F.: OCRA radiometric cloud fractions for GOME-2 on MetOp-A/B, Atmos. Meas. Tech., 9, 2357–2379, doi:10.5194/amt-9-2357-2016, 2016.

Marshak, A., and Davis, A.B. (eds.): 3D Radiative Transfer in Cloudy Atmospheres, Series Physics of Earth and Space Environments. Springer-Verlag, Berlin, Heidelberg, 2005.

Munro, R., Lang, R., Klaes, D., Poli, G., Retscher, C., Lindstrot, R., Huckle, R., Lacan, A., Grzegorski, M., Holdak, A., Kokhanovsky, A., Livschitz, J., and Eisinger, M.: The GOME-2 instrument on the Metop series of satellites: instrument design, calibration, and level 1 data processing – an overview, Atmos. Meas. Tech., 9, 1279–1301, doi:10.5194/amt-9-1279-2016, 2016.

Pedergnana, M., et al., Sentinel-5 precursor/TROPOMI – Level 2 Product User Manual – Cloud Properties, S5P-L2-DLR-PUM-400I available at: https://sentinel.esa.int/web/sentinel/technical-guides/sentinel-5p/appendices/references and http://www.tropomi.eu/documents/level-2-products, 2016.

Rozanov, V., and A. Kokhanovsky. Semi-analytical cloud retrieval algorithm as applied to the cloud top altitude and the cloud geometrical thickness determination from top-of-atmosphere reflectance measurements in the oxygen A-band, J. Geophys. Res., 109, D05202, doi: 10.1029/2003JD004104, 2004.

Schreier F. and B. Schimpf, A new efficient line-by-line code for high resolution atmospheric radiation computations incl. derivatives, in IRS 2000: Current Problems in Atmospheric Radiation, W. L. Smith and Y. Timofeyev, Eds. Hampton, VA, USA: A. Deepak Publishing, pp. 381–384, 2001.

Schreier F., Optimized implementations of rational approximations for the Voigt and complex error function. J. Quant. Spectrosc. Radiat. Transf., 112, 1010–1025, 2011.

Schuessler, O., D. Loyola, A. Doicu, and R. Spurr, Information Content in the Oxygen A-band for the Retrieval of Macrophysical Cloud Parameters, IEEE Trans. Geosci. Remote Sens., 52(6), 2014.

Atmospheric
Measurement
Techniques
Discussions

Sihler H., et al: Clouds, in: Richter, A., et al.: S5P/TROPOMI Science Verification Report; issue: 2.1, URL: https://sentinel.esa.int/web/sentinel/user-guides/sentinel-5p-tropomi/document-library, 2015.

Spurr, R. J. D. VLIDORT: A linearized pseudo-spherical vector discrete ordinate radiative transfer code for forward model and retrieval studies in multilayer multiple scattering media, J. Quant. Spectrosc. Radiat. Transf., 102, 316-42,

5   10.1016/j.jqsrt.2006.05.005, 2006.

Stammes, P., Sneep, M., de Haan J. F., Veefkind, J. P., Wang, P., and Levelt, P. F.: Effective cloud fractions from the Ozone Monitoring Instrument: Theoretical framework and validation, J. Geophys. Res., 113, D16S38, doi:10.1029/2007JD008820, 2008.

Theys, N., De Smedt, I., Yu, H., Danckaert, T., van Gent, J., Hörmann, C., Wagner, T., Hedelt, P., Bauer, H., Romahn, F.,

10 Pedergnana, M., Loyola, D., and Van Roozendael, M.: Sulfur dioxide retrievals from TROPOMI onboard Sentinel-5 Precursor: Algorithm Theoretical Basis, Atmos. Meas. Tech. Discuss., doi:10.5194/amt-2016-309, in review, 2016.

Torres, O., Tanskanen, A., Veihelman, B., Ahn, C., Braak, R., Bhartia, P.K., Veefkind, P., and Levelt, P.: Aerosols and surface UV products from OMI observations: An overview. J. Geophys. Res., 112, D24S47, doi:10.1029/2007JD008809, 2007.

15 Van Roozendael, M., Loyola, D., Spurr, R., Balis, D., Lambert, J-C., Livschitz, Y., Valks, P., Ruppert, T., Kenter, P., Fayt, C., and Zehner C.: Ten years of GOME/ERS-2 total ozone data: the new GOME Data Processor (GDP) Version 4: I. Algorithm Description, J. Geophys Res., doi: 10.1029/2005JD006375, 2006.

Vasilkov, A., J. Joiner, R. Spurr, P. K. Bhartia, P. Levelt, and G. Stephens, Evaluation of the OMI cloud pressures derived from rotational Raman scattering by comparisons with other satellite data and radiative transfer simulations, J. Geophys.

20 Res., 113, D15S19, doi:10.1029/2007JD008689, 2008.

Veefkind, J.P., Aben, I., McMullan, K., Förster, H., de Vries, J., Otter, G., Claas, J., Eskes, H.J., de Haan, J.F., Kleipool, Q., van Weele, M., Hasekamp, O., Hoogeven, R., Landgraf, J., Snel, R., Tol, P., Ingmann, P., Voors, R., Kruizinga, B., Vink, R., Visser, H., and Levelt, P.F.: TROPOMI on the ESA Sentinel-5 Precursor: A GMES mission for global observations of the atmospheric composition for climate, air quality and ozone layer applications, Remote Sensing of Environment,

25 doi:10.1016/j.rse.2011.09.027, 2012.

Veefkind, J.P., de Haan, J. F., Sneep, M., and Levelt, P. F.: Improvements to the OMI O2–O2 operational cloud algorithm and comparisons with ground-based radar–lidar observations, Atmos. Meas. Tech., 9, 6035-6049, doi:10.5194/amt-9-6035-2016, 2016.

Wagner, T., S. Beirle, T. Deutschmann, M. Grzegorski, and U. Platt, Wagner, T., Beirle, S., Deutschmann, T., Grzegorski, M., and Platt, U., Dependence of cloud properties derived from spectrally resolved visible satellite observations on surface temperature, Atmos. Chem. Phys., 8, 2299-2312, doi:10.5194/acp-8-2299–2008, 2008.

Wang, J., W.B. Rossow, and Y. Zhang, Cloud Vertical Structure and Its Variations from a 20-Yr Global Rawinsonde Dataset, J. Clim, 13, Issue 17, 2000.

Wang P., P. Stammes, R. van der A, G. Pinardi, M. van Roozendael, FRESCO+: an improved O_2 A-band cloud retrieval algorithm for tropospheric trace gas retrievals, Atmos. Chem. Phys., 8, 6565-6576, 2008.

Atmospheric
Measurement
Techniques
Discussions
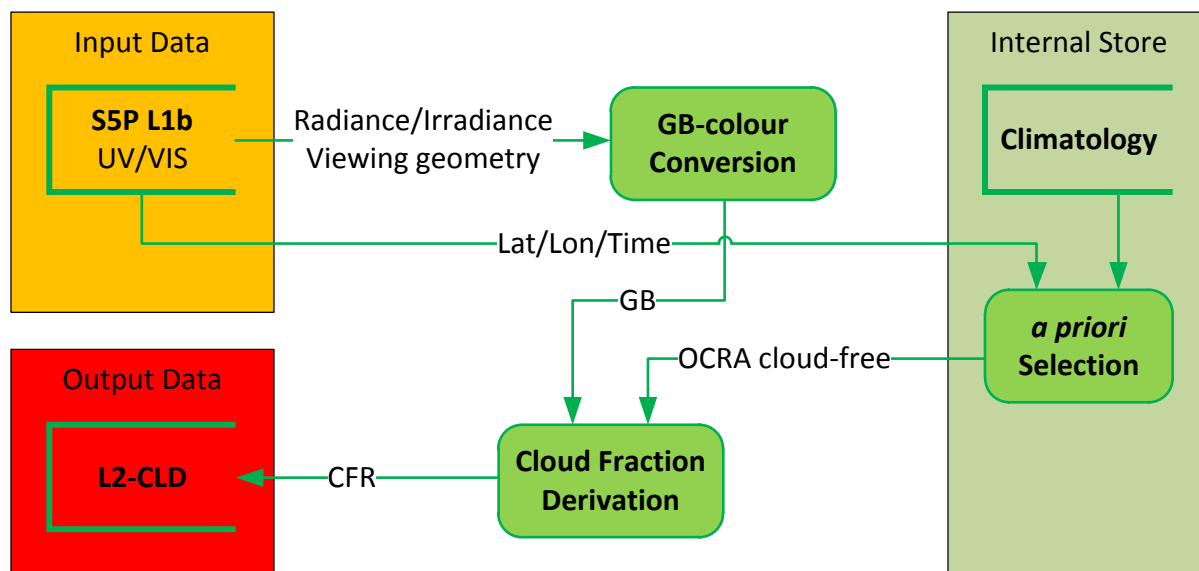
Figure 1: Flow diagram for the OCRA algorithm for the retrieval of the radiometric cloud fraction (CFR).

Atmospheric
Measurement
Techniques
Discussions
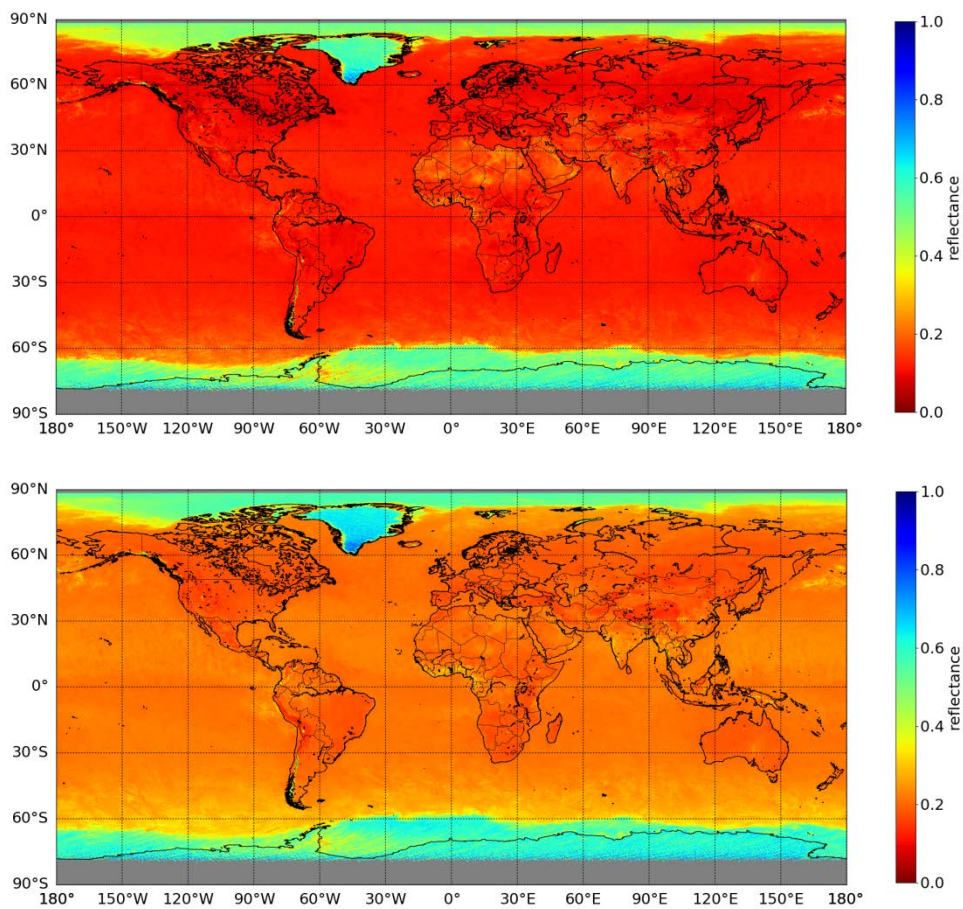
5   **Figure 2: OCRA cloud-free background for G (top) and B (bottom) reflectances calculated using OMI data from August.**

Atmospheric
Measurement
Techniques
Discussions
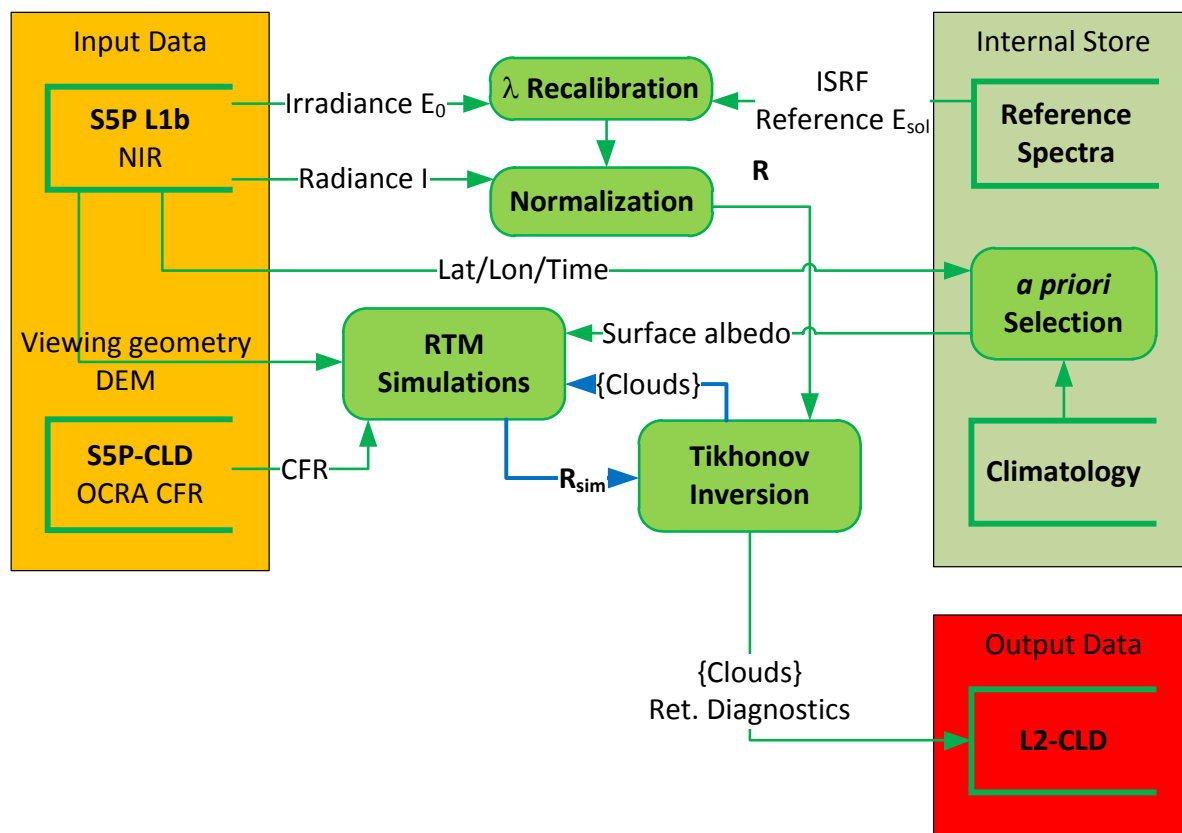
Figure 3: Flow diagram for the ROCINN algorithm for retrieval of cloud properties. The blue arrows mark an iterative loop.

5

Atmospheric
Measurement
Techniques

Discussions
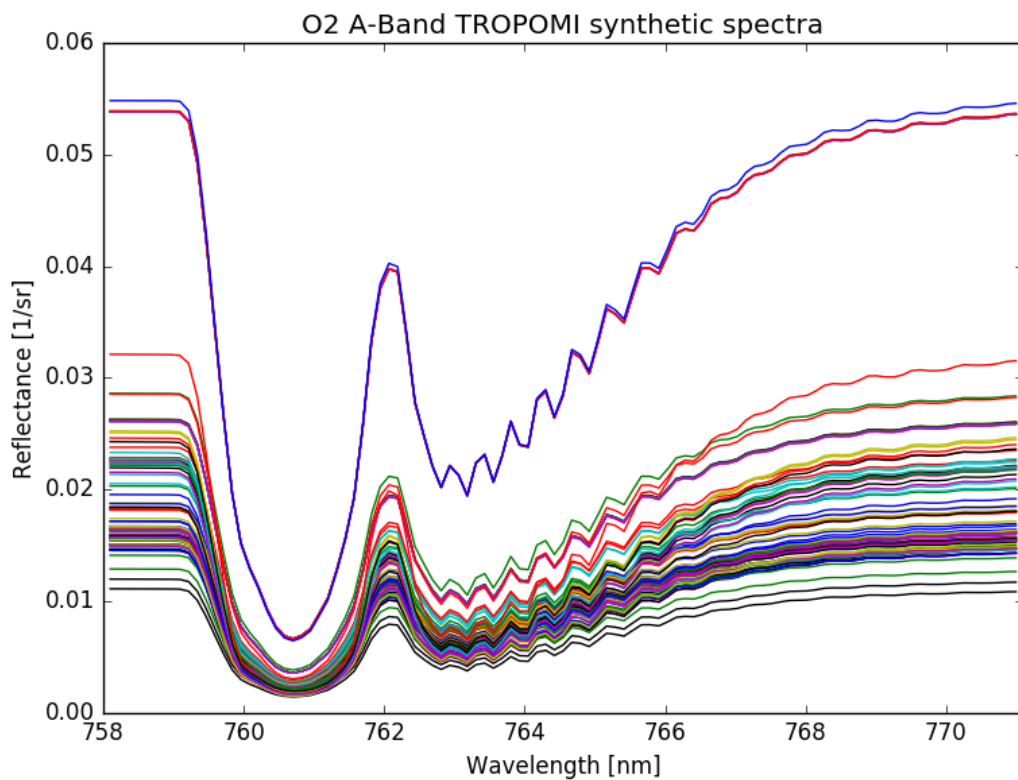
Figure 4: Synthetic Oxygen A-band TROPOMI spectra for different cloud scenarios.

5
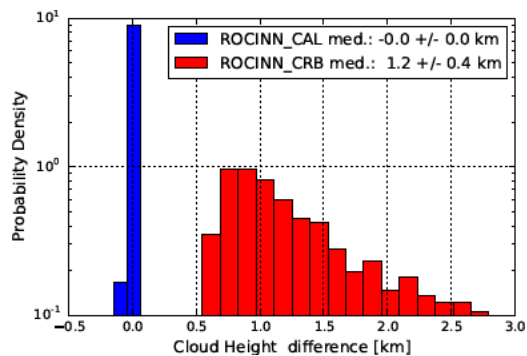
Figure 5: Histogram of the differences between the simulated spectra and the cloud height retrievals from ROCINN_CAL and ROCINN_CRB.
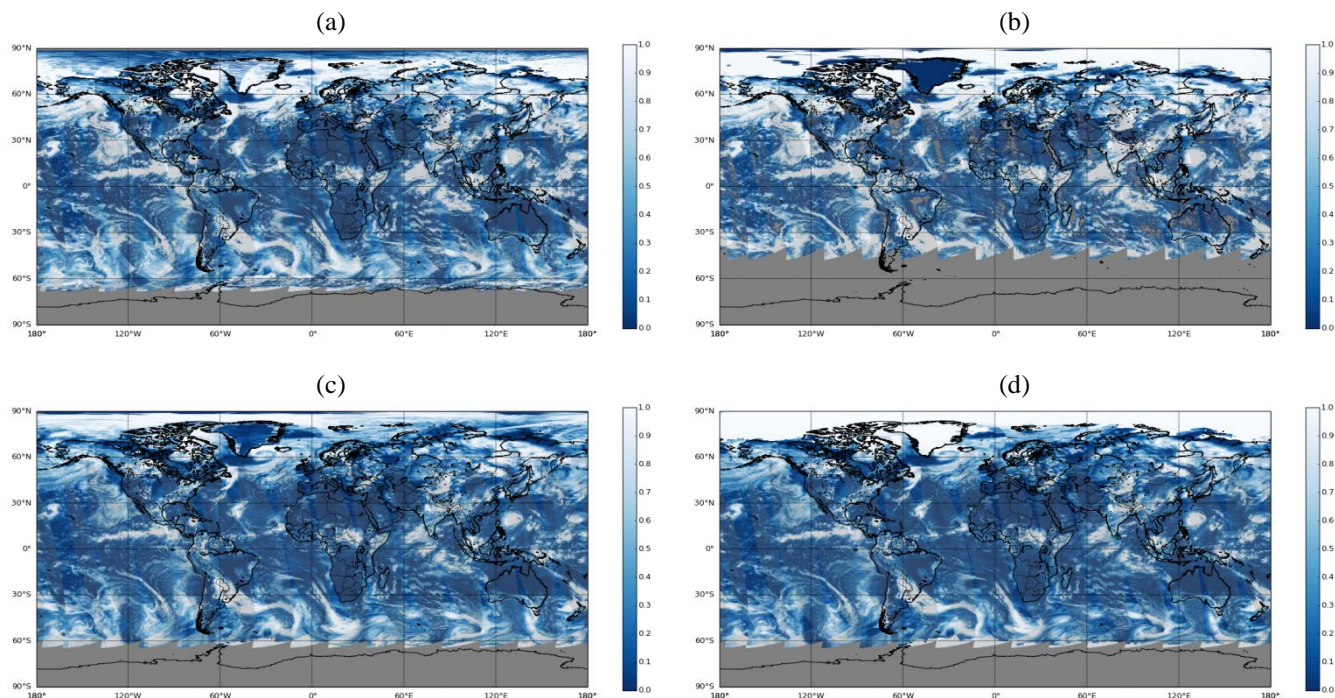
5
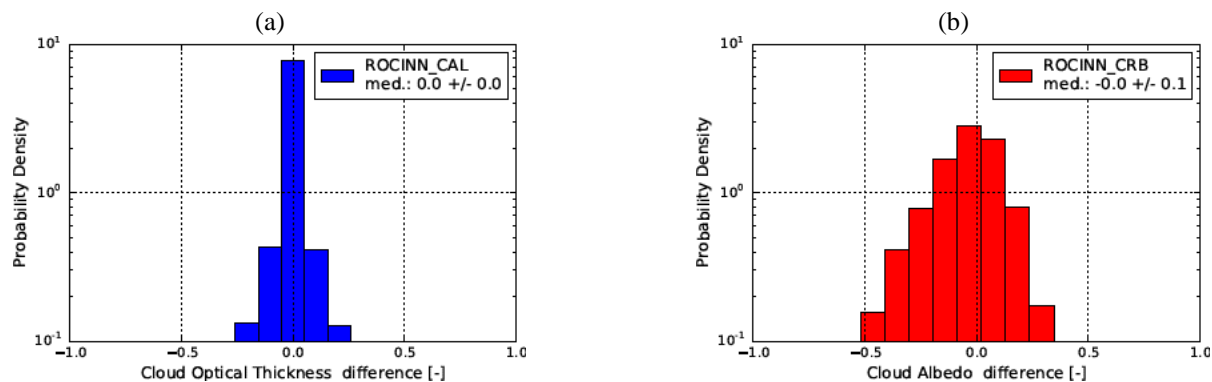
Figure 6: Histogram of the differences between the simulated spectra and (a) the cloud optical thickness retrievals from ROCINN_CAL and (b) the cloud albedo retrievals from ROCINN_CRB.

5

(a)　　　　　　　　　　　　　　　　　　　　　(b)

(c)　　　　　　　　　　　　　　　　　　　　　(d)

Figure 7: Cloud fraction retrieved with (a) OCRA, (b) OMAERUV, (c) OMCLDO2, and (d) OMCLDRR from OMI measurements on July 16th, 2005.
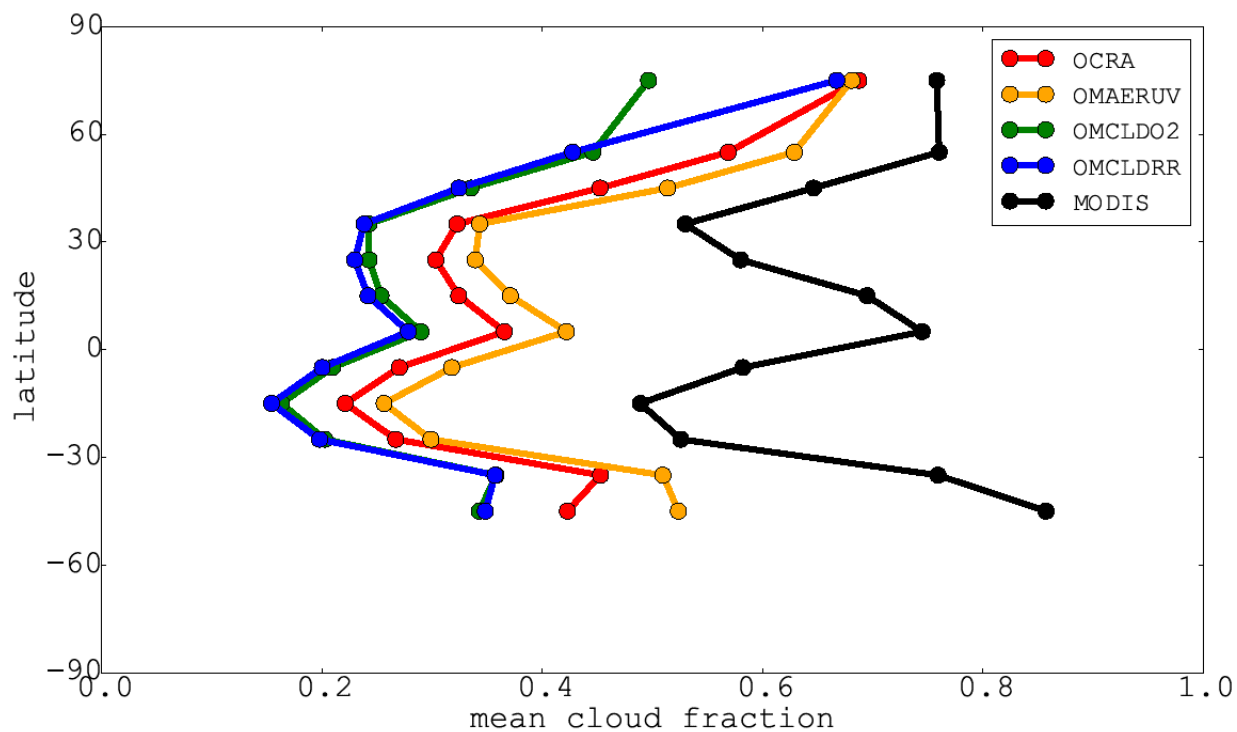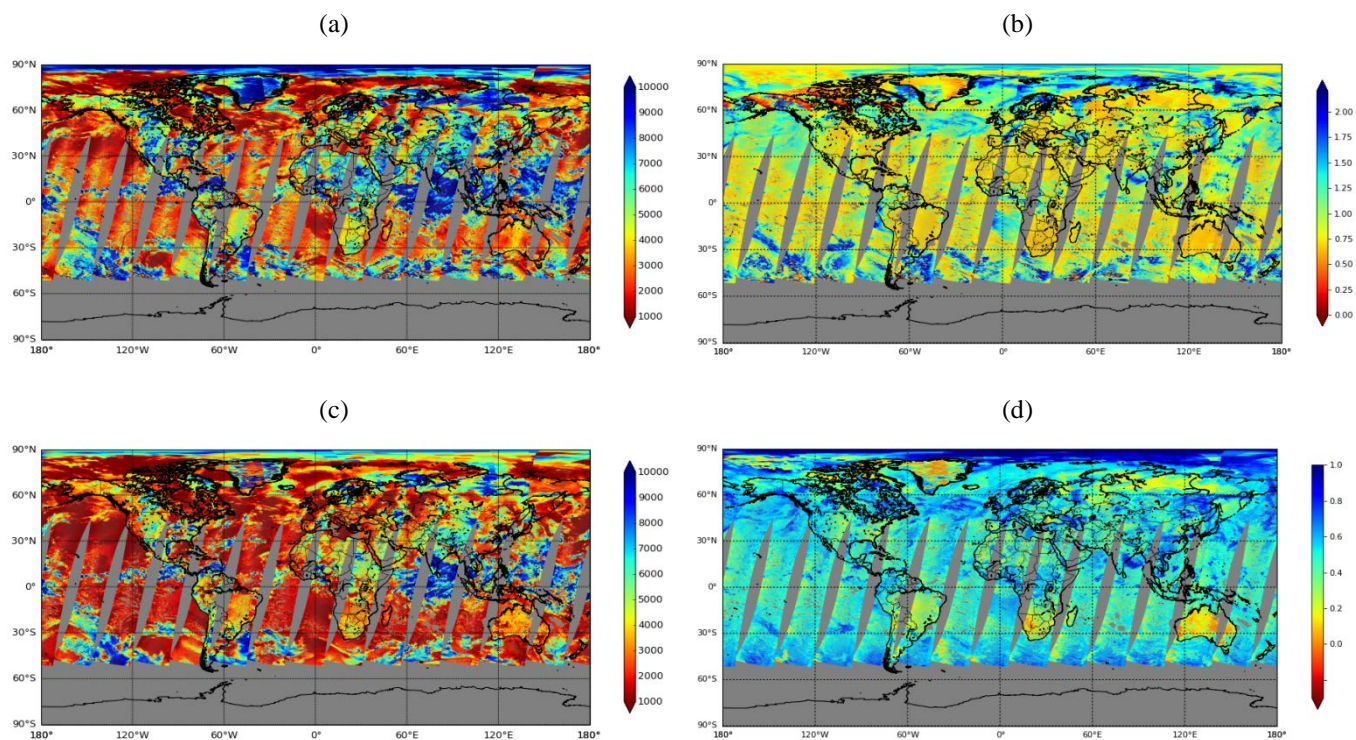
5

Figure 8: Comparison of cloud fraction zonal means for results from the four OMI algorithms as seen in Figure 7 and from the MODIS measurements regridded to the corresponding OMI ground pixels.

5

Atmospheric
Measurement
Techniques
Open Access
Discussions
EGU

(a)   (b)

(c)   (d)

Figure 9: Cloud top height (a) and cloud optical thickness (b) retrieved with ROCINN_CAL, cloud height (c) and cloud albedo (d) retrieved with ROCINN_CRB from GOME-2A measurements on July 1st, 2012. The cloud height is displayed in meters and a logarithmic scale is used for the optical thickness.

5
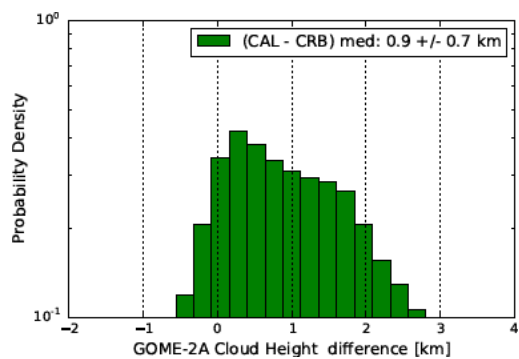
Figure 10: Histogram of the differences between the GOME-2A cloud heights derived from ROCINN_CAL and ROCINN_CRB as seen in Figure 9.

5